Available online at www.sciencedirect.com
ScienceDirect
Journal of Molecular Graphics and Modelling 26 (2008) 834–844
Journal of Molecular Graphics and Modelling
www.elsevier.com/locate/JMGM

Molecular modeling of histamine H3 receptor and QSAR studies on arylbenzofuran derived H3 antagonists

Siavoush Dastmalchi [a,b,c,*], Maryam Hamzeh-Mivehroud [b], Taravat Ghafourian [c,d], Hossain Hamzeiy [a]

[a] School of Pharmacy, Tabriz University of Medical Sciences, Daneshgah Street, Tabriz 51664, Iran
[b] Biotechnology Research Center, Tabriz University of Medical Sciences, Tabriz, Iran
[c] Drug Applied Research Center, Tabriz University of Medical Sciences, Tabriz, Iran
[d] Medway School of Pharmacy, Universities of Kent and Greenwich, Kent, England, United Kingdom

Received 22 November 2006; received in revised form 9 May 2007; accepted 10 May 2007
Available online 16 May 2007

Abstract

Histamine H3 receptors are presynaptic autoreceptors found in both central and peripheral nervous systems of many species. The central effects of these receptors suggest a potential therapeutic role for their antagonists in treatment of several neurological disorders such as epilepsy, schizophrenia, Alzheimer's and Parkinson's diseases. The purpose of this study was to identify the structural requirements for H3 antagonistic activity via quantitative structure–activity relationship (QSAR) studies and receptor modeling/docking techniques. A combination of partial least squares (PLS) and genetic algorithm (GA) was used in the QSAR approach to select the structural descriptors relevant to the receptor binding affinity of a series of 58 H3 antagonists. The descriptors were selected out of a pool of >1000 descriptors calculated by DRAGON, Hyperchem and ACD labs suite of programs. The resulting QSAR models for rat and human H3 binding affinities were validated using different strategies. QSAR models generated in the current work suggested the role of charge transfer interactions in the ligand–receptor interaction verified using the molecular modeling of the receptor and docking two antagonists to the binding site. The 3D model of human H3 receptor was built based on bovine rhodopsin structure and evaluated by molecular dynamics (MD) simulation in a mixed water–vacuum–water environment. The results were indicative of the stability of the model relating the observed structural changes during the MD simulation to the suggested ligand–receptor interactions. The results of this investigation are expected to be useful in the process of design and development of new potent H3 receptor antagonists.

Keywords: Histamine H3 receptor; GPCR; Molecular modeling; QSAR; Docking

1. Introduction

Histamine as an aminergic neurotransmitter (Scheme 1) modulates many physiological processes in the central nervous system (CNS) and peripheral nervous system (PNS) of human and animals [1,2]. Histamine exerts its physiological effects via four distinct G-protein coupled receptors (H1–H4).

Its stimulant effect on H1 receptor leads to immediate hypersensitivity reaction upon IgE mediated release from mast cells. Histamine is also an important regulator of gastric acid secretion through its action upon H2 receptors expressed in parietal cells. The newly discovered H4 receptor found in the immune cells, suggests a role in regulating inflammatory responses [3]. H3 receptor identified in 1983 [4,5], is a presynaptically autoreceptor located in the CNS and in the PNS of many species [6]. It regulates the synthesis and release of histamine by a negative feedback mechanism. On non-histaminergic neurons, H3-heteroreceptors modulate the release of several neurotransmitters such as glutamate, acethylcholine, noradrenaline, dopamine, GABA and serotonin [1,6,7]. The H3 receptors have recently gained attention for their potential role in modulating cognitive, psychiatric, appetitive, allergic and other physiological processes [8] and there is much recent interest in finding potent and efficacious

* Corresponding author at: School of Pharmacy, Tabriz University of Medical Sciences, Daneshgah Street, Tabriz 51664, Iran. Tel.: +98 411 337 2250 1x216; fax: +98 411 334 4798.
E-mail addresses: dastmalchi.s@tbzmed.ac.ir, siavoush11@yahoo.com (S. Dastmalchi).

1093-3263/$ – see front matter © 2007 Elsevier Inc. All rights reserved.
doi:10.1016/j.jmgm.2007.05.002

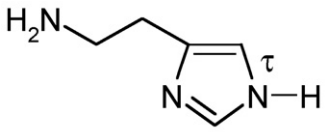

Scheme 1.

H3 receptor antagonists to treat related diseases. Blockade of the histamine H3 autoreceptors by antagonists interrupts a negative feedback mechanism and leads to increased levels of histamine and other neurotransmitters. The central effects of the H3 receptor antagonists suggest a potential therapeutic role for the treatment of several diseases and neurological disorders such as epilepsy, obesity, arousal, attention-deficit hyperactivity disorder (ADHD], schizophrenia, Alzheimer's and Parkinson's diseases [5,9–11]. Recent evidence supports the idea that the combination of an H1 antagonist with an H3 antagonist acts as a nasal decongestant [12]. The increasing interest in the therapeutic potential of H3 agonist or antagonist is driving current medicinal chemistry efforts to identify potent and selective therapeutic agents with improved clinical safety.

The advent of new technologies and developments in the areas of biology and the interface between biology and chemistry in recent years has led to a profound change in the discovery and development of drugs. Rational drug discovery process today takes advantage of the underlying medicinal chemical basis of the observed biological activity and designs new compounds targeted at producing enhanced biological activity. This has been made possible through computational techniques such as receptor modeling/docking and quantitative structure–activity relationships (QSAR) studies on the ligands. The aim of the present investigation was to rationalize H3 binding affinities of a set of antagonists through the use of QSAR and receptor modeling/docking techniques, in order to ultimately aid design and discovery of new H3 antagonists.

2. Methodology

2.1. QSAR studies

In the present study, a dataset of 58 arylbenzofuran derivatives (Table 1) for which H3 receptor binding affinities were reported in the literature [13] was used. The binding affinities (K_i) to rat cortical and human clonal H3 receptors were converted to molar units and after being transformed using

Table 1
Chemical structures and molecular parameters of the arylbenzofuran derivatives used in the study

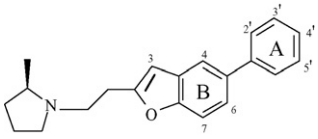

Compound	Benzofuran substituent	Phenyl substituent	E_{HOMO}	log D (pH 7.4)	$Mor_{19\ V}$	$Mor_{30\ M}$	$Mor_{18\ U}$	MAXDP	PSA
p1	H	4′-CN	−8.901	2.15	1.178	0.225	−1.277	3.99	40.17
p2[a]	H	3′-CN	−8.876	2.91	1.022	0.224	−1.249	5.19	52.53
p3[a]	H	4′-F	−8.730	2.76	0.972	0.162	−1.561	4.73	25.61
p4	H	3′-F	−8.798	2.85	1.001	0.217	−1.153	2.55	36.61
p5[b]	H	4′-Cl	−8.725	3.40	0.965	0.151	−1.441	4.29	16.38
p6	H	3′-Cl	−8.783	3.39	0.897	0.208	−1.587	2.56	16.38
p7	H	2′-Cl	−8.711	3.31	0.871	0.223	−1.485	5.82	16.38
p8	H	4′-CF3	−8.939	3.80	1.017	0.326	−1.385	4.46	16.38
p9[a,b]	H	3′-CF4	−8.894	3.80	1.077	0.292	−1.252	2.54	16.38
p10[a,b]	H	4′-Me	−8.578	3.28	1.028	0.114	−1.700	3.08	16.38
p11[a]	H	3′-Me	−8.630	3.28	1.095	0.123	−1.240	2.55	36.61
p12	H	2′-Me	−8.674	3.28	1.066	0.201	−1.470	2.60	33.45
p13[a]	H	4′-OCF3	−8.855	3.68	0.919	0.422	−1.371	4.18	16.38
p14	H	3′-OCF3	−8.852	3.63	0.981	0.519	−1.291	2.54	16.38
p15[a]	H	4′-OMe	−8.449	2.64	0.991	0.112	−1.322	2.53	25.61
p16	H	3′-OMe	−8.631	2.59	1.089	0.159	−1.791	3.07	40.17
p17[b]	H	2′-OMe	−8.433	2.49	1.019	0.171	−1.204	2.53	16.38
p18	H	3′-Cl, 4′-Cl	−8.839	3.84	0.932	0.12	−1.339	2.55	16.38
p19	H	3′-Cl, 5′-Cl	−8.870	3.98	0.865	0.194	−1.249	5.43	40.17
p20[b]	H	3′-Me, 4′-Me	−8.526	3.74	1.244	0.045	−1.444	2.53	25.61
p21	H	3′-Me, 5′-Me	−8.600	3.74	1.260	0.081	−1.326	4.58	40.17
p22	H	4′-COOMe	−8.860	2.70	1.015	0.116	−1.523	4.96	16.38
p23[a]	H	3′-C(O)Me	−8.751	2.27	1.197	0.041	−1.205	4.63	88.64
p24	H	4′-CH2OH	−8.595	1.64	0.978	0.114	−1.344	2.92	33.45
p25[a]	H	3′-CH2OH	−8.652	1.64	0.958	0.206	−1.337	2.95	40.17
p26	H	4′-Br	−8.789	3.73	0.954	0.286	−1.344	2.55	16.38
p27	H	4′-CN, 2′-Me	−8.880	2.61	1.136	0.299	−1.301	3.05	36.61
p28	H	4′-CN, 3′-Me	−8.870	2.61	1.263	0.257	−1.085	3.08	40.17

Table 1 (*Continued*)

Compound	Benzofuran substituent	Phenyl substituent	E_{HOMO}	log *D* (pH 7.4)	$Mor_{19\ V}$	$Mor_{30\ M}$	$Mor_{18\ U}$	MAXDP	PSA
p29	H	4′-CN, 3′-F	−8.997	1.98	0.997	0.263	−1.018	2.98	33.45
p30	7-F	4′-CN	−9.034	2.24	1.030	0.304	−1.541	5.36	48.97
p31	7-Me	4′-CN	−8.857	2.61	1.131	0.241	−1.362	2.97	36.61
p32[a]	6-Me	4′-CN	−8.760	2.61	1.005	0.260	−1.307	3.01	37.97
p33	H	3′-CH(OH)Me	−8.604	1.98	1.012	0.113	−1.36	3.10	40.17
p34	H	3′-C(OH)Me2	−8.560	2.33	1.255	0.186	−1.36	5.39	85.48
p35[a,b]	H	3′-COOH	−8.832	2.77	1.037	0.253	−1.34	2.57	16.38
p36	H	3′-C(O)N(Me)OMe	−8.782	2.04	1.064	0.020	−1.277	2.96	37.97
p37[b]	H	3′-C(O)Et	−8.743	2.80	1.376	−0.033	−1.45	5.00	68.41
p38[b]	H	3′-C(O)CH2CHMe2	−8.745	3.68	1.518	−0.002	−1.521	3.93	40.17
p39	H	3′-C(O)-(3″-F)C6H4	−8.802	3.64	1.113	0.267	−1.25	2.52	25.61
p40[a]	H	3′-CHO	−8.845	2.25	1.058	0.109	−1.247	2.59	40.17
p41	H	3′-C(=NOH)Me	−8.686	2.27	1.209	0.131	−1.281	2.94	40.17
p42[b]	H	3′-C(=NOMe)Me	−8.667	2.80	1.280	0.024	−1.314	3.33	37.97
p43	H	3′-C(=NOEt)Me	−8.656	3.33	1.256	0.116	−1.313	2.62	25.61
p44[b]	H	3′-C(=NO-Bu)Me	−8.642	4.02	1.451	0.147	−1.315	2.58	16.38
p45	H	4′-C(O)-c-Pr	−8.810	2.73	1.314	0.035	−1.454	5.44	33.45
p46	H	3′-C(O)-c-Pr	−8.735	2.64	1.410	−0.037	−1.005	4.28	53.31
p47	3-I	4′-CN	−9.042	3.18	1.035	0.208	−1.557	4.74	33.45
p48	3-Cl	4′-CN	−8.951	2.75	0.966	0.103	−1.361	3.82	33.45
p49	3-Cl, 6-Cl	4′-CN	−8.991	3.21	0.713	0.089	−1.315	2.97	45.92
p50	3-Br	4′-CN	−9.006	2.92	1.160	0.209	−1.252	6.54	40.17
p51	3-Br	4′-CN, 3′-Me	−8.989	3.38	1.270	0.286	−1.472	3.17	53.68
p52[a]	3-Ph	4′-CN	−8.682	3.91	0.831	0.386	−2.101	3.09	40.17
p53[b]	3-(3″,5″-DiMeC6H3)	4′-CN	−8.614	4.83	1.104	0.328	−2.218	3.13	40.17
p54[b]	3-(3″-Pyridyl)	4′-CN	−8.812	2.62	0.909	0.317	−1.507	3.13	40.17
p55[b]	3-(2″-Furyl)	4′-CN	−8.450	3.22	1.319	0.243	−1.131	2.52	16.38
p56[a]	3-(3″-Thienyl)	4′-CN	−8.497	3.59	1.043	−0.001	−1.195	5.08	42.68
p57	3-(3″(2″CHO)Thienyl)	4′-CN	−8.787	2.41	1.048	0.055	−1.231	5.89	33.45
p58[b]	3-(3″(2″CH2OH)-Thienyl)	4′-CN	−8.785	2.40	1.129	0.152	−1.558	3.05	40.17

[a] Test compounds from human data sets.
[b] Test compounds from rat data sets.

$-\log(K_i)$, the resulting pK_i values were used in QSAR analyses (Tables 2 and 3).

The 3D structures of the ligands were generated using the Built Optimum option of Hyperchem software (version 7.0), and subsequently energy minimized using MM+ force field [14]. Then, the structures were fully optimized based on the semiemperical method, using AM1 level of theory [15]. Hyperchem, Dragon (version 3.0) and ACDlabs (version 6.00) suite of programs were employed to calculate the molecular descriptors. HOMO and LUMO energies, molar refractivity, hydration energy, log *P*, dipole moment, surface area and total energy were calculated using Hyperchem. From 1481 different 1D, 2D and 3D molecular descriptors calculated by Dragon software descriptors having less than 0.95 correlation were retained for further analyses [16]. Other descriptors such as log *D* at different pH values, pK_a, molar volume, parachor, density, surface tension and Hansch substituent hydrophobicity constant (π) were computed using ACDlabs software.

Purpose of the descriptor selection procedure is to select the minimum number of appropriate structural parameters for describing the biological activity. This will reduce the risk of chance correlations and overfitting to the training set [17]. PLS is a well-known multivariate method, which gives a stepwise solution for a regression model. This method is preferable for large data sets. It extracts principal component-like latent variables from original independent variables (predictor variables) and dependent variables (response variables). GA is a simulation method mimicking some of the processes observed in natural evolution and has been successfully applied to feature selection in QSAR analyses [18,19]. In this investigation data reduction was initially carried using PLS coupled genetic algorithm (GA-PLS) of Riccardo Leardi using MATLAB software (version7.0) with the following setup: population size, 30; probability of mutation, 0.01; probability of cross-over, 0.5; number of runs, 100. As a result, about 10% of many descriptors (>1000) calculated by DRAGON, Hyperchem and ACDlabs suite of programs were selected [20,21]. The reduced data set was then subjected to stepwise regression analysis to further select a limited number of descriptors significantly contributing to the prediction of activity H3 binding affinity (less than 1 descriptor per 10 compounds was selected).

The predictive power of the models was assessed using leave-one-out cross-validation method [16], as well as performing the internal validation procedure as outlined below. The compounds were randomly divided into the training and test sets consisting of 44 and 14 compounds, for rat and human data sets, respectively. For this selection, the compounds were sorted based on their biological activities and the selection was done randomly throughout entire range of the activity. The test set compounds chosen in this study are indicated in both Tables 1 and 4. The data for training set compounds were used

Table 2
Observed binding affinities[a], $pK_{i(obs)}$, of the substituted arylbenzofurans to the cloned human H3 receptors expressed stably in C6 cells

Compound	$pK_{i(obs)}$ [a]	$pK_{i(calc)}$	$pK_{i(pred)LOO}$	Compound	$pK_{i(obs)}$ [a]	$pK_{i(calc)}$	$pK_{i(pred)LOO}$
p1	9.347	9.461	9.471	p30	9.367	9.329	9.324
p2	9.569	8.854	8.833	p31	8.959	9.068	9.073
p3	8.495	8.708	8.715	p32	9.114	8.690	8.673
p4	8.658	8.723	8.724	p33	9.357	8.991	8.956
p5	8.201	8.403	8.413	p34	9.602	8.907	8.827
p6	8.301	8.323	8.324	p35	7.824	8.802	8.832
p7	8.276	8.164	8.156	p36	9.208	9.543	9.573
p8	8.244	8.343	8.351	p37	9.638	9.600	9.595
p9	8.409	8.398	8.398	p38	9.167	9.300	9.331
p10	8.102	8.336	8.351	p39	8.585	8.397	8.388
p11	8.569	8.501	8.498	p40	9.398	9.380	9.379
p12	8.387	8.397	8.397	p41	9.31	9.220	9.215
p13	8.119	7.933	7.912	p42	9.377	9.227	9.217
p14	7.959	7.843	7.817	p43	8.495	8.742	8.754
p15	8.041	8.358	8.400	p44	8.367	8.571	8.608
p16	8.921	8.757	8.750	p45	9.585	9.549	9.546
p17	7.824	8.322	8.398	p46	9.678	9.713	9.717
p18	8.444	8.425	8.423	p47	9.292	9.084	9.064
p19	8.301	8.189	8.174	p48	9.409	9.235	9.219
p20	8.229	8.422	8.444	p49	9.081	8.796	8.705
p21	8.444	8.514	8.520	p50	9.538	9.297	9.277
p22	8.721	9.125	9.144	p51	8.886	9.036	9.056
p23	10.076	9.501	9.467	p52	7.678	7.455	7.421
p24	9.056	9.093	9.099	p53	7.222	7.342	7.369
p25	9.31	8.998	8.952	p54	7.886	8.552	8.597
p26	8.114	8.091	8.090	p55	8.553	8.242	8.179
p27	8.699	9.006	9.028	p56	8.678	8.275	8.209
p28	9.553	9.229	9.199	p57	9.137	9.286	9.295
p29	9.194	9.421	9.448	p58	8.721	9.203	9.219

$pK_{i(calc)}$ and $pK_{i(pred)LOO}$ denote the calculated binding affinities based on Eq. (1) and the predicted values in leave-one-out cross-validation study.
[a] Data taken from Gfesser et al. [13].

to train the QSAR models in order to predict the biological activity (pK_i) of the test set compounds. Absolute percentage errors (APE) of predictions were calculated for each data point and averaged using the following equations:

$$\mathrm{APE} = \frac{|pK_{i(\mathrm{pred})} - pK_{i(\mathrm{obs})}|}{pK_{i(\mathrm{obs})}} \times 100$$

$$\mathrm{MAPE} = \frac{\sum_{i=1}^{n} \mathrm{APE}}{n}$$

where $pK_{i(pred)}$ and $pK_{i(obs)}$ are the predicted and observed binding affinities and n denotes the number of compounds. MAPE is the mean of APE values. Moreover, standard deviation of error of prediction (SDEP) was calculated to assess the distribution of error levels for rat and human data using the following equation:

$$\mathrm{SDEP} = \sqrt{\frac{\sum_{i=1}^{N} (y_i - \tilde{y}_i)^2}{n}}$$

2.2. Molecular modeling

Structural coordinates for all proteins used in this study were retrieved from the Protein Data Bank at the Research Collaboratory for Structural Bioinformatics (http://www.RCSB.org) [22]. The BLAST search engine which is publicly available at National Center for Biotechnology Information (NCBI) was used to find the homologous proteins with known structures as the templates for comparative modeling of H3 receptor [23]. The only suitable template for GPCR receptors is bovine rhodopsin (PDB code of 1U19) [24]. To align the sequence of human H3 receptor with that of bovine rhodopsin, the CLUSTALW program was used from its web site at http://www2.ebi.ac.uk/CLUSTALW [25]. The alignment was adjusted manually based on the conserved key residues of GPCRs suggested by Baldwin et al. [26]. The Swiss Pdb Viewer (DeepView version, 3.7) program was downloaded from ExPASY proteomics server of the Swiss Institute of Bioinformatics and used as a viewing program as well as to perform the modeling job. DeepView was used to thread the sequence of Human H3 receptor onto the structure of template (bovine rhodopsin) based on the final alignment and to submit the modeling job to the SWISS-MODEL server (http://www.expasy.org/swissmod/SWISSMODEL.HTML) [27].

The structure file for the ensemble consisting of the protein main chain and histamine or an antagonist in the appropriate format recognizable to GROMACS program was prepared using pdb2gmx command in GROMACS package and PRODRG server at http://davapc1.bioch.dundee.ac.uk/programs/prodrg/prodrg.html [28]. Gaussian molecular orbital program applying 6-31G* basis set was used to calculate

Table 3
Observed binding affinities[a], $pK_{i(obs)}$, of the substituted arylbenzofurans to the rat H3 receptors from the membrane of rat cortex

Compound	$pK_{i(obs)}$[a]	$pK_{i(calc)}$	$pK_{i(pred)LOO}$	Compound	$pK_{i(obs)}$[a]	$pK_{i(calc)}$	$pK_{i(pred)LOO}$
p1	8.495	8.369	8.363	p30	8.244	8.404	8.423
p2	8.602	8.407	8.392	p31	7.796	7.903	7.906
p3	7.187	7.596	7.633	p32	8.377	7.984	7.972
p4	7.770	7.936	7.947	p33	8.553	8.289	8.270
p5	7.086	7.168	7.173	p34	8.886	9.282	9.384
p6	7.319	6.874	6.845	p35	7.180	7.390	7.403
p7	7.620	7.319	7.262	p36	8.310	8.276	8.274
p8	6.824	7.045	7.065	p37	8.638	8.588	8.582
p9	7.022	6.979	6.975	p38	7.721	7.421	7.405
p10	6.796	6.875	6.882	p39	7.276	7.246	7.243
p11	7.523	7.655	7.663	p40	8.481	8.213	8.197
p12	7.481	7.388	7.384	p41	8.509	8.207	8.193
p13	6.699	7.088	7.116	p42	8.347	7.919	7.910
p14	6.886	7.025	7.034	p43	7.292	7.345	7.347
p15	7.252	7.654	7.673	p44	7.387	6.822	6.769
p16	7.638	7.610	7.607	p45	8.194	7.937	7.914
p17	7.119	7.640	7.684	p46	8.602	8.682	8.690
p18	6.959	6.883	6.877	p47	8.076	7.564	7.537
p19	7.620	7.668	7.676	p48	8.432	7.855	7.842
p20	7.187	7.025	7.016	p49	8.013	7.854	7.845
p21	7.721	7.630	7.623	p50	8.469	8.274	8.240
p22	7.377	7.490	7.507	p51	7.796	7.813	7.814
p23	9.357	9.441	9.467	p52	6.409	6.709	6.804
p24	8.387	8.308	8.298	p53	6.076	6.173	6.230
p25	8.553	8.456	8.445	p54	7.745	7.858	7.862
p26	6.523	6.931	6.958	p55	7.377	7.361	7.359
p27	7.509	7.966	7.979	p56	7.387	7.919	7.978
p28	8.585	8.236	8.214	p57	8.237	8.332	8.346
p29	8.032	8.445	8.488	p58	7.699	7.907	7.922

$pK_{i(calc)}$ and $pK_{i(pred)LOO}$ denote the calculated binding affinities based on Eq. (2) and the predicted values using leave-one-out cross-validation study.
[a] Data taken from Gfesser et al. [13].

Mulliken partial atomic charges [29] for histamine and the other two antagonists using Hyperchem software. The calculated charges were used to edit the topology files generated by the PRODRG server. The initial model from SWISS-MODEL was used for the purpose of Docking. Flexible docking of H3 receptor was carried out using histamine and two selected H3 antagonists, namely p1 and p23 in GOLD program (version 2.0) [30,31] running on Windows XP. Docking was performed by applying a hydrogen binding constraint between N^{τ} nitrogen atom of imidazole ring from histamine and the oxygen atom of Glu^{206} side chain from protein. The second constraint imposed on the system was a distance constraint

Table 4
Predicted values of binding affinities for test set compounds in human and rat dataset obtained from Eqs. (3) and (4)

Compound	Human		APE	Compound	Rat		APE
	$pK_{i(obs)}$	$pK_{i(pred)}$			$pK_{i(obs)}$	$pK_{i(pred)}$	
p2	9.569	8.823	7.80	p5	7.086	7.166	1.12
p3	8.495	8.665	2.00	p9	7.022	6.918	1.48
p9	8.409	8.381	0.34	p10	6.796	6.904	1.59
p10	8.102	8.295	2.38	p17	7.119	7.689	8.01
p11	8.569	8.466	1.20	p20	7.187	6.972	2.99
p13	8.119	7.910	2.58	p35	7.18	7.427	3.44
p15	8.041	8.307	3.31	p37	8.638	8.554	0.97
p23	10.076	9.467	6.05	p38	7.721	7.361	4.67
p25	9.310	8.949	3.88	p42	8.347	7.918	5.14
p32	9.114	8.655	5.03	p44	7.387	6.748	8.65
p35	7.824	8.772	12.11	p53	6.076	6.078	0.03
p40	9.398	9.340	0.61	p54	7.745	7.885	1.81
p52	7.678	7.420	3.36	p55	7.377	7.338	0.53
p56	8.678	8.228	5.18	p58	7.699	7.960	3.39
MAPE			3.99	MAPE			3.13

MAPE is the mean of absolute percentage error (APE).

(1.5–3.5 Å) between nitrogen atom at the side chain of histamine and carboxylic carbon atom of Asp^{114} residue of the protein. This is to simulate the presence of an ionic interaction between oppositely charged nitrogen atom and carboxylate groups in histamine and the receptor, respectively. Such a distance constraint is also employed between pyrrolidine nitrogen atom of antagonists and the carboxylate group from the receptor. Acceptable formats for protein and ligand coordinate files used in this study were *pdb* and Tripos *mol2*, respectively. Geometric center of the residues, Asp^{80}, Asp^{114}, Tyr^{189}, Glu^{206}, Tyr^{374} (identified to be part of the binding site) was calculated and set as the center of the active site [32–37]. The ligand–receptor complexes resulting from the docking calculation were placed in a box of water using algorithms implemented in the GROMACS. To simulate the hydrophobic nature of the environment in which the transmembrane (TM) region of the receptor is located, a slab of water molecules corresponding to this region was removed. This effectively produced two parallel layers of water separated by a vacuum layer of 29 Å thickness. Although for a realistic simulation, the lipid bilayers consist of mixture of different lipid molecules are to be used, but such a system demands enormous computational resources. Therefore, avoiding explicit lipid molecules is preferable unless one is interested in protein–membrane interactions. The resulting partially solvated ligand–receptor complex was energy minimized using GROMACS program (version 3.1.1) under conjugate gradient and periodic boundary condition [38,39].

A molecular dynamics (MD) simulation was carried out for 1 ns after initially equilibrating water molecules for 50 ps where the non-water components were fixed. During the MD simulation every 1 ps the actual frame was stored. An average structure was calculated for the models of the ligand–receptor complex generated during the final 0.6 ns of the MD simulation where the root mean square deviation (RMSD) values had already reached the plateau. The average structure was energy minimized under conjugate gradient and periodic boundary condition. The dynamic behaviour and structural changes of the receptor was analyzed by calculating the RMSD values, a commonly used parameter indicating the structural movement, and changes in the elements of the secondary structure of the receptor models during the MD simulation.

3. Results and discussion

The structures of the H3 receptor antagonists used in this study are shown in Table 1. The benzofuran series bear a wide variety of substituents creating a desirable dataset for QSAR analysis. The substituents vary in size and lipophilicity as well as electron directing properties. For a successful QSAR analysis, it is necessary to capture various aspects of chemical information within the data set using a wide range of structural descriptors. However, it has been recognized in various fields of chemometrics that an efficient variable selection as well as reducing the complexity of the model which in turn improves interpretability, enhances the predictive ability [17,19,20]. The large number of descriptors used in this study contained graph theoretical, molecular mechanical and quantum mechanical descriptors as well as partition and distribution coefficients. Application of GA-PLS algorithm for variable selection resulted in the following QSAR models for human and rat H3 antagonists:

$$\begin{aligned} \mathrm{p}K_{i(\mathrm{human})} &= -7.30(\pm2.67) - 1.88(\pm0.30)E_{\mathrm{HOMO}} \\ &\quad - 0.48(\pm0.07)\log D_{\mathrm{pH\,7.4}} + 1.26(\pm0.29)\mathrm{Mor}_{19\,\mathrm{V}} \\ &\quad - 1.93(\pm0.44)\mathrm{Mor}_{30\,\mathrm{M}}, \\ n &= 58,\ r^2 = 0.754,\ F = 40.7,\ \mathrm{S.E.} = 0.317,\ q^2_{\mathrm{LOO}} = 0.71 \end{aligned} \quad (1)$$

$$\begin{aligned} \mathrm{p}K_{i(\mathrm{rat})} &= 9.32(\pm0.31) + 0.99(\pm0.19)\mathrm{Mor}_{18\,\mathrm{U}} \\ &\quad - 0.47(\pm0.07)\log D_{\mathrm{pH\,7.4}} + 0.10(\pm0.04)\mathrm{MAXDP} \\ &\quad + 0.02(\pm0.003)\mathrm{PSA}, \\ n &= 58,\ r^2 = 0.840,\ F = 69.8,\ \mathrm{S.E.} = 0.288,\ q^2_{\mathrm{LOO}} = 0.81 \end{aligned} \quad (2)$$

Eqs. (1) and (2) describe the ligand binding affinities to human and rat H3 receptors, respectively, based on the four selected molecular parameters for each correlation. The molecular descriptors in the equations are the energy of highest occupied molecular orbital (E_{HOMO}), apparent distribution coefficient at pH 7.4 ($\log D_{\mathrm{pH\ 7.4}}$) and 3D-MoRSE descriptors ($\mathrm{Mor}_{19\ \mathrm{V}}$ and $\mathrm{Mor}_{30\ \mathrm{M}}$) for human data set and $\log D_{\mathrm{pH\ 7.4}}$, 3D-MoRSE descriptor ($\mathrm{Mor}_{18\ \mathrm{U}}$), MAXDP topological descriptor and fragment-based polar surface area (PSA) for the rat data set. Number of data (n), squared correlation coefficient (r^2), F-value (F) and standard error (S.E.) are model statistics.

The observed and calculated H3 binding affinities of the ligands ($\mathrm{p}K_{i(\mathrm{obs})}$ and $\mathrm{p}K_{i(\mathrm{calc})}$), as well as their predicted activities using the leave-one-out cross-validation method ($\mathrm{p}K_{i(\mathrm{pred})}$) are listed in Tables 2 and 3 for human and rat data, respectively. The q^2_{LOO} values (Eqs. (1) and (2)) indicate a good predictive power for both of the models. Furthermore, the SDEP values of 0.328 and 0.298 for human and rat data sets show the narrow distribution of error indicative of good performances of the models for all the chemicals in the datasets.

In order to evaluate further the predictive power of the QSAR model, compounds were randomly divided into test and training sets containing 14 and 44 chemicals, respectively. Eqs. (3) and (4) are the models obtained for the training set compounds for human and rat datasets, respectively, using the molecular descriptors selected in the previous step.

$$\begin{aligned} \mathrm{p}K_{i(\mathrm{human})} &= -7.64(\pm2.62) - 1.90(\pm0.29)E_{\mathrm{HOMO}} \\ &\quad - 0.48(\pm0.06)\log D_{\mathrm{pH\,7.4}} + 1.34(\pm0.26)\mathrm{Mor}_{19\,\mathrm{V}} \\ &\quad - 1.87(\pm0.41)\mathrm{Mor}_{30\,\mathrm{M}}, \\ n &= 44,\ r^2 = 0.813,\ F = 42.3,\ \mathrm{S.E.} = 0.266 \end{aligned} \quad (3)$$

$$\begin{aligned} \mathrm{p}K_{i(\mathrm{rat})} &= 9.49(\pm0.41) + 0.80(\pm0.24)\mathrm{Mor}_{18\,\mathrm{U}} \\ &\quad - 0.56(\pm0.08)\log D_{\mathrm{pH\,7.4}} + 0.10(\pm0.04)\mathrm{MAXDP} \\ &\quad + 0.02(\pm0.003)\mathrm{PSA}, \\ n &= 44,\ r^2 = 0.837,\ F = 50.0,\ \mathrm{S.E.} = 0.288 \end{aligned} \quad (4)$$

To further evaluate the validity of the model, the available binding values (human and rat data) were randomly assigned to the compounds shown in Table 1 and then the descriptor selection procedure and statistical analyses were performed as described in Section 2. In this way, none of the molecular parameters selected for the real situations (Eqs. (1) and (2)) were among the first 30 descriptors. For human dataset, the r^2 values for the randomized MLR equations using first 4 and 5 selected parameters were 0.37 and 0.29, respectively. In the case of rat dataset, the r^2 values were also very small, i.e., 0.30 and 0.24 for randomized MLR equations using first 4 and 5 selected parameters, respectively. The lack of correlations demonstrated by these results indicates that the molecular features shown in Eqs. (1) and (2) were not selected by chance.

Finally, the affinity data were randomly assigned to the compounds and the squared correlation coefficient between the calculated pK_i and the randomized-observed pK_i values was obtained by MLR using variables of Eqs. (1) and (2) for the human and rat data, respectively. The randomization and determination of r^2 was repeated 10 times for both human and rat data. The mean r^2 values obtained by this procedure were 0.070 and 0.134 for human and rat data, respectively.

Table 4 shows the H3 binding affinities of the test set compounds predicted by Eqs. (3) and (4) and the observed values. The mean absolute percentage error (MAPE) of the predictions for human and rat binding data are 3.99 and 3.13, respectively, which indicate a good predictive power for the models. Fig. 1 is the plot between observed and predicted pK_i values for the test compounds, showing a better correlation for the rat data.

Based on the Eq. (1), the binding affinities show a negative correlation with E_{HOMO}, that is, the lower the E_{HOMO} values for a molecule the stronger it binds to the receptor. This in turn indicates the possibility of charge transfer interaction between ligands and the receptor. Considering that replacement of E_{HOMO} term with the sum of the Hammett electronic constants for the substituents on the phenyl A ring, $\sum\sigma_{Ph}$, in Eq. (1) leads to a statistically significant QSAR with a positive coefficient for

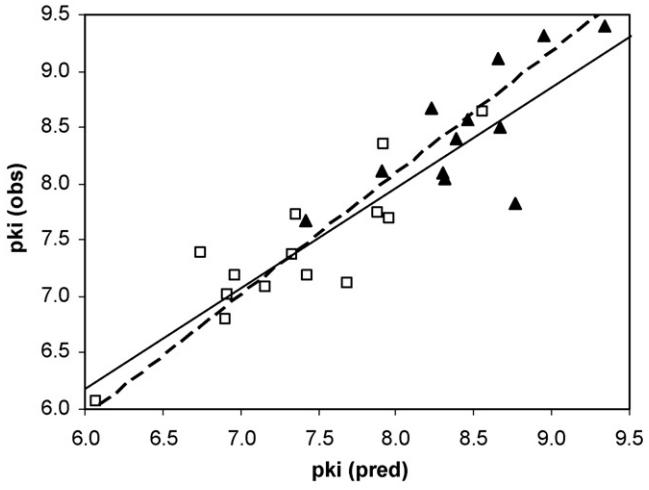

Fig. 1. Plot of the observed vs. calculated pK_i values for the binding affinities to the H3 receptors. The solid and dashed lines represent the best fit lines for the human (▲) and rat (□) data points, respectively.

$\sum\sigma_{Ph}$ (r^2 of the model is 0.676), it can be assumed that this interaction is mediated through unoccupied orbital of the benzofuran attached phenyl group (A ring) of the ligands and HOMO of aromatic residues from the receptor. In other words, the electronegative nature of the substituents on ring A lead to an electron deficient aromatic system capable of charge transfer interaction. Although the energy of lowest unoccupied molecular orbital (E_{LUMO}) has not been selected as one of the molecular descriptors in the QSAR model, however, the straight relationship between E_{HOMO} and E_{LUMO} energies allows us to suggest that the charge transfer interaction could happen between the lowest unoccupied orbital of the ligands and the highest occupied molecular orbital of the receptor site. The correlation between these two energies for the compounds under investigation is 0.65 which improves to 0.91 after excluding p52, p53, p55, p56 and p57 from the correlation. The negative model constant for log $D_{pH\ 7.4}$ indicates an inverse relationship between pK_i and the relative hydrophobicity of the compounds. The average log $D_{pH\ 7.4}$ values for these compounds at pH 7.4 and for their neutral forms are 2.98 and 5.56, respectively, indicating a generally lipophilic nature for these molecules. As the chemicals share a general benzofuran system and the only difference between them is in the substituents, the negative coefficient of log $D_{pH\ 7.4}$ in the equation shows a higher receptor binding affinity for the ligands with hydrophilic substituents. Further investigation of the relationship between sum of the hydrophobicity constants for the substituents on the A phenyl ring and benzofuran moiety ($\sum\pi_{Ph,Bf}$ values) and the biological activity revealed an inverse correlation. Such a correlation was also noted based on the structure activity studies on the compounds by Gfesser et al. [13]. Replacement of log $D_{pH\ 7.4}$ with $\sum\pi_{Ph,Bf}$ in Eq. (1) resulted in a new model with a similar correlation coefficient. Both $Mor_{19\ V}$ and $Mor_{30\ M}$ belong to 3D-MoRSE descriptors which are developed based on the idea of obtaining information from 3D atomic coordinates by the transform used in electron diffraction studies [40,41]. Unfortunately, it is difficult to relate these descriptors to a specific physical property of molecules and the interpretation is somehow vague. However, these descriptors represent 3D structures of the molecules and based on the weighting used in the calculations they are related to the volume ($Mor_{19\ V}$) or mass ($Mor_{30\ M}$) of molecules.

Eq. (2) correlates the rat H3 receptor binding affinities of the compounds in Table 1 to $Mor_{18\ U}$, log $D_{pH\ 7.4}$, MAXDP and PSA molecular descriptors. $Mor_{18\ U}$, an unweighted 3D-MoRSE descriptor, is related to the volume of the molecule. Thus, the bigger the antagonist molecule (or, to be more precise, the bigger the substituents of the molecule) the higher the affinity to the rat H3 receptor. Binding affinities to rat H3 receptors are affected by the lipophilicity (log $D_{pH\ 7.4}$) of the compounds in the same way as it was described above for the human receptors. The positive model constant for MAXDP in Eq. (2) indicates a positive relationship between electrophilicity of the polar moieties of the molecule and the binding affinities to the receptor [42]. This could be related to the charge transfer capability of the molecule and be considered as a descriptor equivalent to E_{HOMO} in Eq. (1). The other term in the

model is PSA which positively affects the binding affinities. Such a positive relationship may explain the presence of polar interactions between ligand and receptor, such as hydrogen bonding. The higher the PSA values, the greater the observed affinities.

In order to investigate further the interaction between the ligands and the human H3 receptor in a 3D fashion, a homology model of the receptor was built using rhodopsin molecule as the template. The sequence alignment between bovine rhodopsin and human H3 receptor was generated using ClustalW method and then further improved manually according to the known key conserved residues of the rhodopsin family of proteins (see Fig. 2 for details). After threading the sequence of human H3 receptor onto the structure of rhodopsin guided by the alignment, the initial model structure was sent to SWISS-MODEL server for structure optimization. This model shows the conserved disulfide bond between Cys^{107} located at the end of first extracellular loop and Cys^{188} in the second extracellular loop [37]. The model received from the server was used to dock histamine, an agonist, and p1 and p23 antagonists into the binding site. The docking calculations were constrained based on the well-known interaction between protonated side chain amine group present in biological amines, such as dopamine, adrenaline and histamine, and a negatively charged residue, that is, Asp or Glu residues in the third helix of related GPCRs corresponding to the location of Asp^{114} in H3 receptor [43]. The other constraint imposed on the system was a hydrogen bonding interaction between N^{τ} imidazole ring of histamine and Glu^{206} from receptor located in transmembrane helix 5 proposed by many investigators [34,36]. A two-dimensional representation of the ligand–receptor interactions is shown in Fig. 3 for the complex of H3 receptor with histamine antagonist p23. In addition to the imposed ionic interaction between Asp^{114} and pyrrolidine N^{1} atom, several other interactions are also evident. The main interactions include one hydrogen bonding and two sets of hydrophobic interactions. The hydrogen bonding interaction is between benzofuran O^{1} atom of p23 and hydroxyl group of Tyr^{189}. The hydrophobic interactions are between core A phenyl ring attached to benzofuran of antagonists and side chains of residues Ala^{122}, Phe^{211}, Val^{214} and Phe^{367}, which form a hydrophobic pocket. According to our model, side chains of residues Phe^{398}, Leu^{401} and Trp^{371} as well as benzene group of Tyr^{189} (not shown in Fig. 3) form the second set of hydrophobic interactions with hydrophobic regions of ethyl pyrrolidine and benzofuran moieties. The hydrogen bonding and hydrophobic interaction between antagonists and receptor are not seen for histamine. The antagonist activity for the ligands in Table 1 may arise from these extra interactions.

The observed interactions proposed by molecular modeling studies are in agreement with those obtained from QSAR studies. According to Eq. (1) for human data set, charge transfer interactions are assumed between unoccupied orbital of the benzofuran or the A phenyl ring of the antagonist ligands with the π systems present in the hydrophobic pockets formed by residues Ala^{122}, Phe^{211}, Val^{214}, Trp^{371}, Phe^{367}, Phe^{398} and Leu^{401}. For instance, the A phenyl ring bearing an electron withdrawing methyl keto group can be considered as an

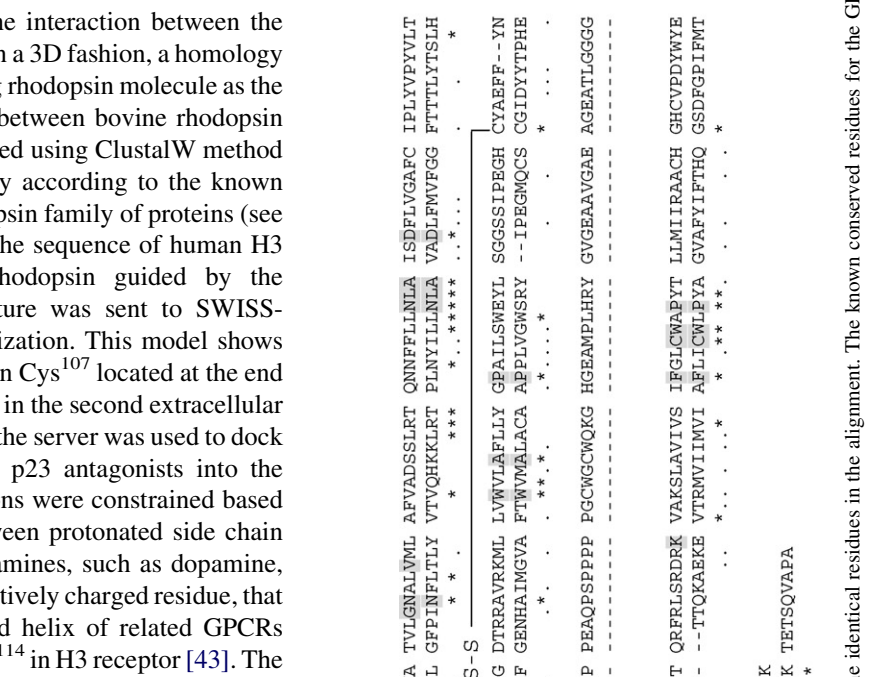

Fig. 2. Sequence alignment between bovine rhodopsin (template) and human H3 receptor. The asterisks denote the identical residues in the alignment. The known conserved residues for the GPCRs suggested by Baldwin et al. [26] are shaded.

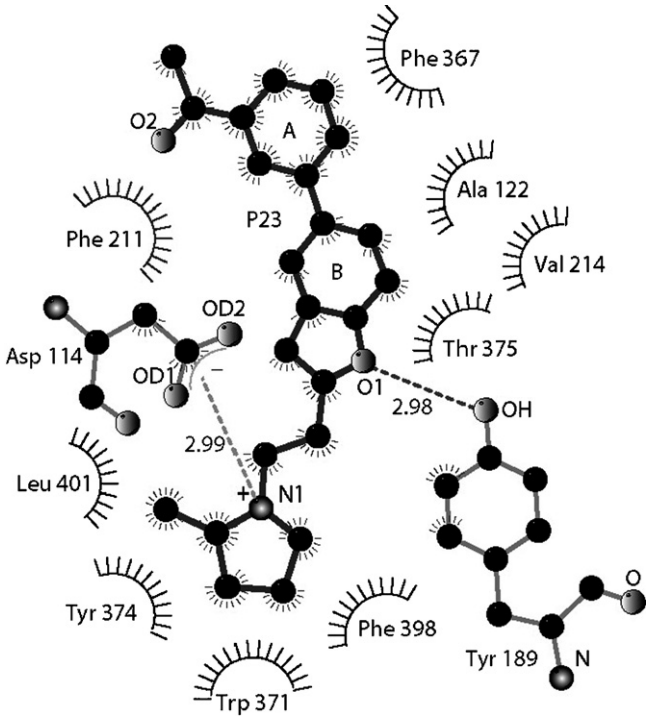

Fig. 3. A two-dimensional representation of the ligand–receptor interactions for the complex of H3 receptor with histamine antagonist p23. The plot was produced using LIGPLOT program. The ionic interaction between Asp^{114} and pyrrolidine N^1 atom of p23 and the hydrogen bonding interaction between benzofuran O^1 atom of p23 and hydroxyl group of Tyr^{189} are indicated with dashed lines.

electron deficient π system which can be involved in charge transfer interactions with the side chains of Phe^{211} and Phe^{367} residues positioned parallel and ∼50° inclined to the plane of the A phenyl ring, respectively.

The structural changes of the H3 receptor model was evaluated during 1 ns MD simulation by calculating the changes of potential energy, RMSD values and the secondary structure content of the model. It can be seen from Fig. 4 that the potential energy of the H3 receptor model without any ligand drops rapidly to its equilibrium value in about 200 ps and in the mean time the RMSD differences of the model relative to its structure at time zero reaches to ∼2.3 Å during the first 50 ps of the MD simulation and then stays constant till 250 ps and after that slowly increases to ∼2.9 Å at the end of 1 ns simulation. These patterns for the changes of potential energy is very similar for the receptor in the presence of the ligands, however, the RMSD value for ligand–receptor complex reaches to the plateau (∼2.9 Å) within the first 200 ps and does not increase afterward. The secondary structure content (number of residues assigned to be in the α-helix, β-sheet, β-bridge and turn secondary structures) of the human H3 receptor model was 244 residues which showed minor changes during MD simulation. The average secondary structure content of the model during the final 0.6 ns of the simulation without any ligand docked into the active site dropped to 220 residues. The corresponding average values for the model in the presence of histamine, p1 and p23 were 224, 226 and 225, respectively. The above-mentioned results are indicative of the stability of the

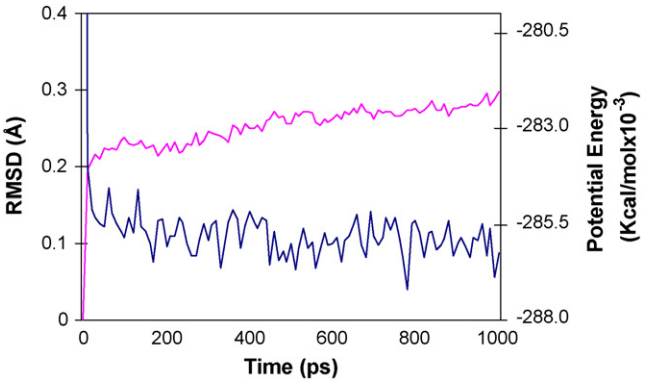

Fig. 4. The RMSD differences of the model trajectories for all backbone atoms and changes of the potential energy during 1 ns molecular simulation for the human H3 receptor model without any ligand in the active site.

human H3 receptor model proposed in this study. At the end of the simulation of models with agonist (histamine) or antagonist (p23), the most appreciable difference between the two complexes was the gross movement of the first half of helix 5 toward the lipid environment (away from the helical bundle center) in the antagonist–receptor complex (Fig. 5). The RMSD value for 14 pairs of C^{α} atoms of residues comprising this part of the helix 5 was 5.33 Å. This movement of the helix 5 was also occurred for H3 model simulated without any ligand. The reason for the lack of movement of helix 5 in the presence of histamine could be the hydrogen bonding interaction between N^{τ} hydrogen of the histamine molecule with Glu^{206} in helix 5. Such an interaction is missing from the antagonist–receptor complexes or receptor alone and could be essential for the agonist activity. From the presented results, it can be concluded that the main commonality between binding sites for H3 antagonists and histamine as an agonist involves negatively charged carboxylic group of Asp^{114} on the third helix of the receptor and a protonated amine group from agoinst/antagonist. In a recent study, Axe et al., proposed that Asp^{114} as well as Glu^{206} on the third and fifth helices, respectively, interact with

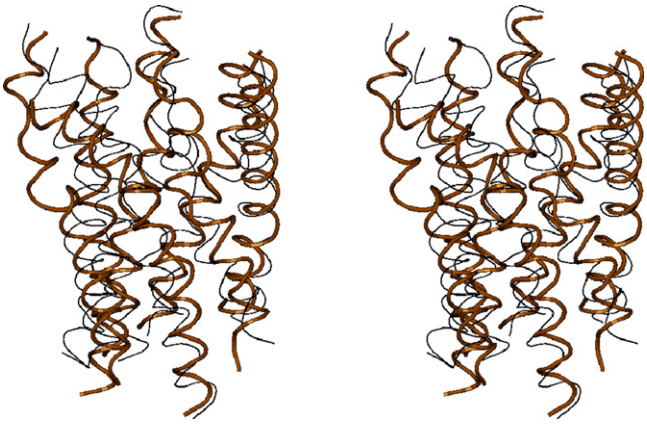

Fig. 5. Comparison of helical portion of human H3 receptor model structures at the end of 1 ns molecular simulation in the presence of histamine and p23. The models were superimposed using 218 carbon alpha atom pairs in the helical regions. The schematic tube representations of the models were produced by VMD program [45]. The light and heavy tubes are the H3 model with histamine and p23, respectively.

antagonists containing two basic groups connected by a hydrophobic region occupying mostly the same region as agonists [44]. However, the results from our docking calculations suggest a slightly different antagonist binding site which may be due to the structural differences between the antagonists used in the current study and those studied by Axe et al.

4. Conclusions

Histamine H3 receptors are involved in many neurological disorders and their antagonists have been suggested to have potential therapeutic importance. In the current study, the molecular features governing the human and rat H3 receptor affinities were investigated using QSAR and ligand–receptor molecular modeling approaches. The ligands consisted of a series of benzofuran derivatives with known antagonistic activities. The molecular features identified via genetic algorithm based partial least square (GA-PLS) method indicated a charge transfer interaction between the electron deficient aromatic system in the ligands and the electron-rich aromatic residues in the receptor. Comparative molecular modeling of human H3 receptor based on the bovine rhodopsin structure followed by docking a number of antagonists to the receptor confirmed the results of the QSAR. This method was able to identify the amino acid residues responsible for the formation of hydrogen bonding (Tyr^{189}) and hydrophobic pockets accommodating the aromatic systems of the ligands. Phenylalanine residues (Phe^{211} and Phe^{367}) were located in the appropriate position of the pocket to act as the charge transfer donor π systems. Furthermore, statistical evaluations of the QSAR models revealed good predictive power with leave-one-out cross-validation q^2 of >0.71. The r^2 values for the correlations between observed and predicted H3-binding affinities of test compounds in human and rat data sets were 0.65 and 0.77, respectively. The results of this investigation are expected to be useful in the process development of new potent H3 receptor antagonists and may also be used in experimental design for site-directed mutational studies on H3 receptor.

Acknowledgment

The authors would like to thank the Research Office at TUOMS for providing the financial support of the current work.

References

[1] K. Takahashi, H. Suwa, T. Ishikawa, H. Kotani, Targeted disruption of H3 receptors results in changes in brain histamine tone leading to an obese phenotype, J. Clin. Invest. 110 (2002) 1791–1799.
[2] B.H.C. Westerink, T.I.F.H. Cremers, J.B. Vries, H. Liefers, N. Tran, P. Boer, Evidence for activation of histamine H3 autoreceptors during handling stress in the prefrontal cortex of the rat, Synapse 43 (2002) 238–243.
[3] M. Cowart, J.K. Pratt, A.O. Stewart, Y.L. Bennani, T.A. Esbenshade, A.A. Hancock, A new class of potent non-imidazole H3 antagonists: 2-aminoethylbenzofuranes, Bioorg. Med. Chem. Lett. 14 (2004) 689–693.
[4] C. Shah, L. McAtee, G. Breitenbucher, D. Rudolph, X. Li, T.W. Lovenberg, C. Mazur, S.J. Wilson, N.I. Carruthers, Novel human histamine H3-receptor antagonists, Bioorg. Med. Chem. Lett. 12 (2002) 3309–3312.
[5] S.C. Turner, T.A. Esbenshade, Y.L. Bennani, A.A. Hancock, A new class of histamine H3-receptor antagonists: Synthesis and Structure-Activity Relationships of 7,8,9,10-tetrahydro-6H-cyclohepta[*b*]quinolines, Bioorg. Med. Chem. Lett. 13 (2003) 2131–2135.
[6] V. Zuliani, F. Bordi, M. Rivara, C. Silva, F. Vacondio, G. Morini, S. Rivara, E. Barocelli, V. Ballabeni, S. Bertoni, F. Magnanini, P.V. Plazzi, The role of HB-donor groups in the heterocyclic polar fragment of H3-antagonist, IL Farmaco 58 (2003) 891–899.
[7] M. Mor, F. Bordi, C. Silva, S. Rivara, V. Zuliani, F. Vacondio, G. Morini, E. Barocelli, V. Ballabeni, M. Impicciatore, P.V. Plazzi, Synthesis and biological assays of new H3-antagonists with imidazole and imidazoline polar groups, IL Farmaco 55 (2000) 27–34.
[8] M. Cowart, R. Faghih, M.P. Curtis, G.A. Gfesser, Y.L. Bennani, L.A. Black, L. Pan, K.C. Marsh, J.P. Sullivan, T.A. Esbenshade, G.B. Fox, A.A. Hancock, 4-(2-[2-(2-(R)-Methylpyrrolidin-1-yl)ethyl]benzofuran-5-yl) benzonitrile and related 2-Aminoethylbeznofuran H3 receptor antagonists potently enhance cognition and attention, J. Med. Chem. 48 (2005) 38–55.
[9] A.A. Hancock, Y.L. Bennani, E.N. Bush, T.A. Esbenshade, R. Faghih, G.B. Fox, P. Jacobson, V. Knourek-Segel, K.M. Krueger, M.E. Nuss, J.B. Pan, R. Shapiro, D.G. Witte, B.B. Yao, Antiobesity effects of A-331440, a novel non-imidazole histamine H3 receptor antagonist, Eur. J. Pharmacol. 487 (2004) 183–197.
[10] R. Faghih, W. Dwight, L. Black, H. Liu, R. Gentles, K. Phelan, T.A. Esbenshade, L. Ireland, T.R. Miller, C.-H. Kang, K.M. Krueger, G.B. Fox, A.A. Hancock, Y.L. Bennani, Structure–activity relationships of non-imidazole H3 receptor ligands. Part 2: Binding preference for D-amino acids motifs, Bioorg. Med. Chem. Lett. 12 (2002) 2035–2037.
[11] S. Grabmann, J. Aplet, W. Sippl, X. Ligneau, P.H.H. Zhao, Y.H. Arrang, J.-M. Ganellin, C.R. Schwartz, J.-C. Schunack, W. Stark H, Imidazole derivatives as a novel class of hybrid compounds with inhibitory Histamine N-Methyltransferase potencies and histamine hH3 receptor affinities, Bioorg. Med. Chem. 11 (2003) 2163–2174.
[12] R. Aslanian, M.W. Mutahi, N.-Y. Shih, K.D. McCormick, J.J. Piwinski, P.C. Ting, M.M. Albanese, M.Y. Berlin, X. Zhu, S.-C. Wong, S.B. Rosenblum, Y. Jiang, R. West, S. She, S.M. Williams, M. Bryant, J.A. Hey, Identification of a novel, orally bioavailable histamine H3 receptor antagonist based on the 4-benzyl-(1*H*-imidazole-4-yl) template, Bioorg. Med. Chem. Lett. 12 (2002) 937–941.
[13] G.A. Gfesser, R. Faghih, Y.L. Bennani, M.P. Curtis, T.A. Esbenshade, A.A. Hancock, M.D. Cowart, Structure–activity relationships of arylbenzofuran H3 receptor antagonists, Bioorg. Med. Chem. Lett. 15 (2005) 2559–2563.
[14] N.L. Allinger, Conformational analysis 130. MM2. A hydrocarbon force field utilizing v1 and v2 torsional terms, J. Am. Chem. Soc. 99 (1977) 8127–8134.
[15] M.J.S. Dewar, W. Thiel, Ground states of molecules.39.MNDO results for molecules containing hydrogen, carbon, nitrogen and oxygen, J. Am. Chem. Soc. 99 (1977) 4907–4917.
[16] R. Todeschini, V. Consonni, Handbook of Molecular Descriptors, Wiley-VCH, Weinheim, 2000.
[17] T. Ghafourian, M.T. Cronin, The impact of variable selection on the modelling of oestrogenicity, SAR QSAR Environ. Res. 16 (2005) 171–190.
[18] K. Tang, T. Li, Combining PLS with GA–GP for QSAR, Chemom. Intl. Lab. Sys. 64 (2002) 55–64.
[19] Z. Daren, QSPR studies of PCBs by the combination of genetic algorithms and PLS analysis, Comput. Chem. 25 (2001) 197–204.
[20] R. Leardi, A. Lupianez, Genetic algorithm applied to feature selection in PLS regression: how and when to use them, Chemolab 41 (1998) 195–207.
[21] R. Leardi, Application of genetic algorithm-PLS for feature selection in spectral data sets, J. Chemometrics 14 (2000) 643–655.
[22] H.M. Berman, J. Westbrook, Z. Feng, G. Gililand, T.N. Bahat, H. Weissig, P.E. Shindyalov, The protein data bank, Nucl. Acids Res. 28 (2000) 235–242.
[23] S.F. Altschul, W. Gish, W. Miller, E.W. Myers, D.J. Lipman, Basic local alignment search tool, J. Mol. Biol. 215 (1990) 403–410.

[24] T. Okada, M. Sugihara, A.N. Bondar, M. Elstner, P. Entel, V. Buss, The retinal conformation and its environment in rhodopsin in light of a new 2.2 A crystal structure, J. Mol. Biol. 342 (2004) 571–583.
[25] J.D. Thompson, D.G. Higgins, T.J. Gibson, CLUSTAL W: improving the sensitivity of progressive multiple sequence alignment through sequence weighting, position-specific gap penalties and weight matrix choice, Nucl. Acids Res. 22 (1994) 4673–4680.
[26] J.M. Baldwin, G.F.X. Schertler, V.M. Unger, An alpha-carbon template for the transmembrane helices in the rhodopsin family of G-protein-coupled receptors, J. Mol. Biol. 272 (1997) 144–164.
[27] N. Guex, M.C. Peitsch, SWISS-MODEL and the Swiss pdb viewer: an environment for comparative protein modelling, Electrophoresis 18 (1997) 2714–2723.
[28] D.M.F. Van Aalten, R. Bywater, J.B.C. Findlay, M. Hendlich, R.W.W. Hooft, G. Vriend, PRODRG, a program for generating molecular topologies and unique molecular descriptors from coordinates of small molecules, J. Comput. Aid. Mol. Des. 10 (1996) 255–262.
[29] R.S. Mulliken, Electronic population analysis on LCAO-MO molecular wave functions. I., J. Chem. Phys. 23 (1955) 1833–1840.
[30] G. Jones, P. Willett, R.C. Glen, Molecular recognition of receptor sites using a genetic algorithm with a description of desolvation, J. Mol. Biol. 245 (1995) 43–53.
[31] G. Jones, P. Willett, R.C. Glen, A.R. Leach, R. Taylor, Development and validation of a genetic algorithm for flexible docking, J. Mol. Biol. 267 (1997) 727–748.
[32] E.S. Huang, Construction of a sequence motif characteristic of aminergic G protein-coupled receptors, Protein Sci. 12 (2003) 1360–1367.
[33] B.B. Yao, C.W. Hutchins, T.L. Carr, S. Cassar, J.N. Masters, Y.L. Bennani, T.A. Esbenshade, A.A. Hancock, Molecular modeling and pharmacological analysis of species-related histamine H3 receptor heterogeneity, Neuropharmacology 44 (2003) 773–786.
[34] A.J. Uveges, D. Kowal, Y. Zhang, T.B. Spangler, J. Dunlop, S. Semus, P.G. Jones, The role of transmembrane helix 5 in agonist binding to the human H3 receptor, J. Pharmacol. Exp. Ther. 301 (2002) 451–458.
[35] I.J.P. De Esch, H. Timmerman, W.M.P.B. Menge, P.H.J. Nederkoorn, A qualitative model for the histamine H3 receptor explaining agonistic and antagonistic activity simultaneously, Arch. Pharm. Pharm. Med. Chem. 333 (2000) 254–260.
[36] S. Lorenzi, M. Mor, F. Bordi, S. Rivara, M. Rivara, G. Morini, S. Bertoni, V. Ballabeni, E. Barocelli, P.V. Plazzi, Validation of a histamine H3 receptor model through structure-activity relationships for classical H3 antagonists, Bioorg. Med. Chem. 13 (2005) 5647–5657.
[37] A.A. Hancock, T.A. Esbenshade, K.M. Krueger, B.B. Yao, Genetic and pharmacological aspects of histamine H3 receptor heterogeneity, Life Sci. 73 (2003) 3043–3072.
[38] H.J.C. Berendsen, D. Van der Spoel, R. Van Drunen, GROMACS: a message-passing parallel molecular dynamics implementation, Comput. Phys. Commun. 91 (1995) 43–56.
[39] E. Lindahl, B. Hess, D. Van der Spoel, GROMACS 3.0: a package for molecular simulation and trajectory analysis, J. Mol. Mod. 7 (2001) 306–317.
[40] J. Schuur, J. Gasteiger, Infrared spectra simulation of substituted benzene derivatives on the basis of a 3D structure representation, Anal. Chem. 69 (1997) 2398–2405.
[41] J. Schuur, P. Selzer, J. Gasteiger, The coding of the three-dimensional structure of molecules by molecular transforms and its application to structure-spectra correlations and studies of biological activity, J. Chem. Inf. Comput. Sci. 36 (1996) 334–344.
[42] P. Gramatica, M. Corradi, V. Consonni, Modelling and prediction of soil sorption coefficients of non-ionic organic pesticides by molecular descriptors, Chemosphere 41 (2000) 763–777.
[43] M. Eilers, V. Hornak, S.O. Smith, J.B. Konopka, Comparison of class A and D G protein-coupled receptors: common features in structure and activation, Biochemistry 44 (2005) 8959–8975.
[44] F.U. Axe, S.D. Bembenek, S. Szalma, Three-dimensional models of histamine H3 receptor antagonist complexes and their pharmacophore, J. Mol. Graph. Model. 24 (2006) 456–464.
[45] W. Humphrey, A. Dalke, K. Schulten, VMD—visual molecular dynamics, J. Mol. Graph. 14 (1996) 33–38.